iScience, Volume *24*

Supplemental Information

A human pluripotent stem cell model for the analysis of metabolic dysfunction in hepatic steatosis

Matthew C. Sinton, Jose Meseguer-Ripolles, Baltasar Lucendo-Villarin, Sara Wernig-Zorc, John P. Thomson, Roderick N. Carter, Marcus J. Lyall, Paul D. Walker, Alpesh Thakker, Richard R. Meehan, Gareth G. Lavery, Nicholas M. Morton, Christian Ludwig, Daniel A. Tennant, David C. Hay, and Amanda J. Drake

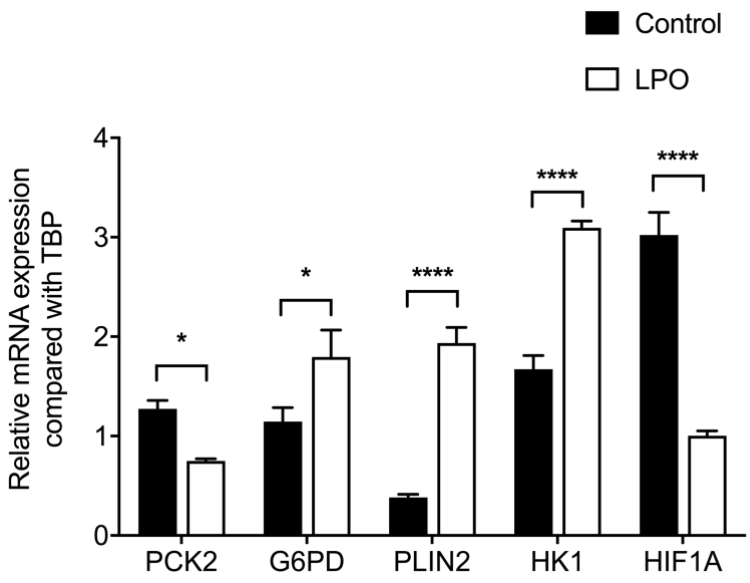

Figure S1. Validation of mRNA sequencing analysis by RT-qPCR. Data were analysed using two-tailed Student t-test and expressed as mean ± SD, *p<0.05, ****p<0.0001. Related to Figure 2.

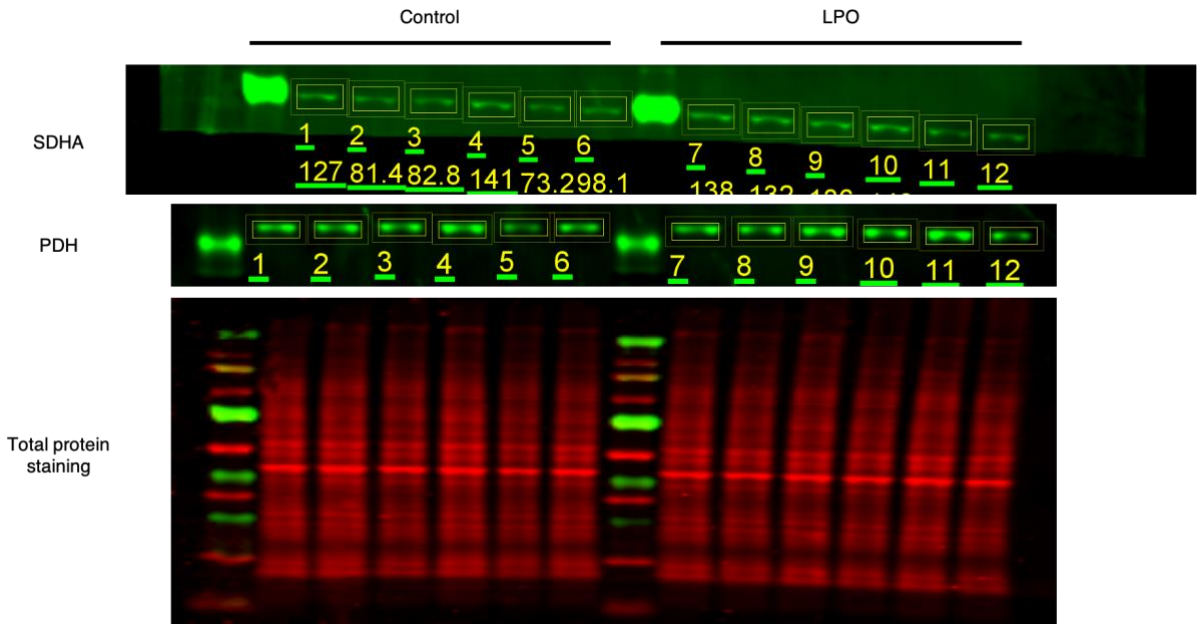

Figure S2. Representative blot of succinate dehydrogenase subunit A (SDHA) and pyruvate dehydrogenase (PDH) α1 and α2 subunits, with total protein staining. Molecular weight band of SDHA = 70 kDa. Molecular weight band of PDh = 38 kDa. Related to Figure 3.

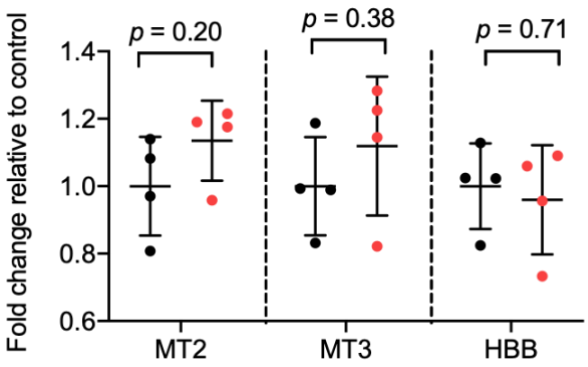

Figure S3. Measurement of mitochondrial (mitochondrial region 2 (MT2); mitochondrial region 3 (MT3)) and nuclear (beta-globin (HBB)) DNA. Data are expressed as mean ± SD. Related to Figure 3.

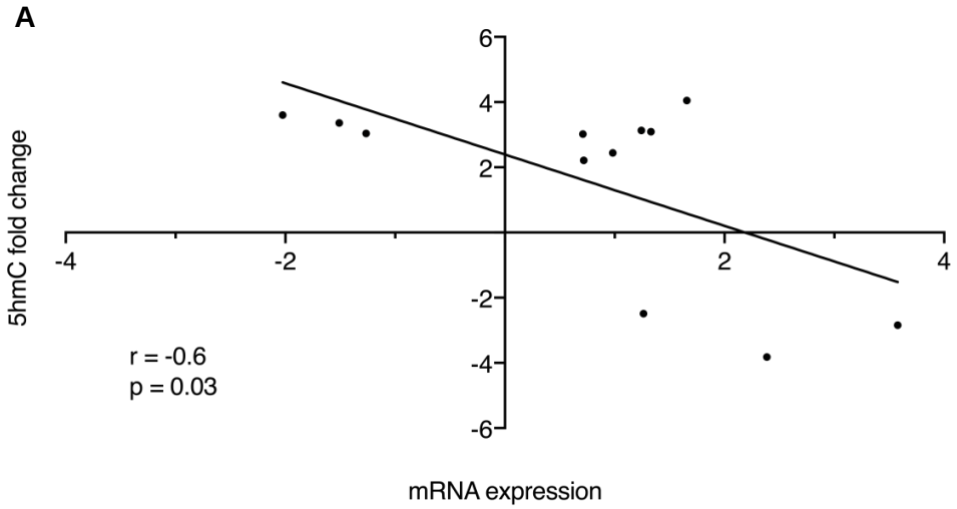

Figure S4. Steatotic HLCs show a moderate negative correlation between promoter 5hmC enrichment and mRNA expression, Related to Figure 7.

Gene	Forward sequence	Reverse sequence	Probe
TBP	GAACATCATGGATCAGAACAACA	ATAGGGATTCCGGGAGTCAT	87
NANOG	ATGCCTCACACGGAGACTGT	CAGGGCTGTCCTGAATAAGC	69
ALB	GTGAGGTTGCTCATCGGTTT	GAGCAAAGGCAATCAACACC	7
HNF4A	AGCAACGGACAGATGTGTGA	TCAGACCCTGAGCCACCT	27
PLIN2	TCAGCTCCATTCTACTGTTCACC	CCTGAATTTTCTGATTGGCACT	72
PLIN4	AGTTCCAAGCCAGGGACAC	TGCTGGGCCTTTTCAATC	1
PLIN5	TACAGTGCAGCCAAGGACAG	CGCACACGCAGTTCTCAG	3
PCK2	CGAAAGCTCCCCAAGTACAA	GCTCTCTACTCGTGCCACATC	20
G6PD	AACAGAGTGAGCCCTTCTTCA	GGAGGCTGCATCATCGTACT	5
PLIN2	TCAGCTCCATTCTACTGTTCACC	CCTGAATTTTCTGATTGGCACT	72
HK1	GACCAAGTTTCTCTCTCAGATCG	CCTAGCTGCTGGAGGATAGC	1
HIF1A	GATAGCAAGACTTTCCTCAGTCG	TGGCTCATATCCCATCAATTC	64

Table S1. Primer pairs and probes used to quantify mRNA expression, Related to Figure 1 and Figure 2.

Gene	Forward Primer	Reverse Primer
MT1	CTCACTCTCACTGCCCAAGA	TGAGAATGAGTGTGAGGCGT
MT2	ACCCACCAATCACATGCCTA	GTGTTACATCGCGCCATCAT
HBB	TGGTGCATCTGACTCCTGAG	TCTCCACATGCCCAGTTTCT

Table S2. Primer pairs used to quantify mitochondrial and nuclear DNA, Related to Figure 3.

Gene	Forward sequence	Reverse sequence
GAPDH promoter – negative control	CGGCTACTAGCGGTTTTACG	AAGAAGATGCGGCTGACTGT
H19 genic – positive control	GATCTCGGCCCTAGTGTGAA	GTGATGTGTGAGCCTGCACT
UBIAD1 genic – positive control	CTCTTCCTCCTCCTCGTCCT	CATCCAGGAACCACAGTCCT

Table S3. Primer sequences for validation of DNA immunoprecipitation protocol, Related to Figure 7.

Pathways with upregulated genes		
Pathway	*Benjamini*	*Genes*
hsa04713: Circadian entrainment	4.20	ADCY4, ADCY2, CACNA1I, GRIN1, GRIA3, PRKG1, PRKCB, KCNJ5, PLCB4, GRIN2D, CACNA1G, RYR1, GNG2, PER3, GNG4, MTNR1A
hsa04724: Glutamatergic synapse	4.15	ADCY4, DLGAP1, ADCY2, GRIK2, GRIN1, GRIK5, GRIN3B, GRIA3, SHANK1, PRKCB, SLC17A7, GLS2, GRM4, PLCB4, GRIN2D, PLA2G4F, GNG2, GNG4, PLA2G4D
hsa04725: Cholinergic synapse	3.59	ADCY4, ACHE, ADCY2, KCNJ12, KCNJ14, PRKCB, KCNJ4, KCNQ4, KCNQ3, CHRM4, PLCB4, GNG2, PIK3R5, GNG4, KCNQ1, CHRNA3
hsa04750: Inflammatory mediator regulation of TRP channels	3.31	ADCY4, ADCY2, TRPM8, TRPV2, ASIC3, ASIC1, PRKCB, PLCB4, PLA2G4F, PIK3R5, ALOX12, NGF, PLA2G4D
hsa05414: Dilated cardiomyopathy	3.26	ADCY4, ADCY2, ADRB1, SGCG, CACNG8, ITGA8, ITGA7, CACNB1, CACNB4, TNNI3, ITGA2B
hsa04911: Insulin secretion	3.23	TRPM4, ADCY4, ADCY2, PLCB4, KCNN1, KCNN3, ATP1A3, RIMS2, PCLO, KCNJ11, PRKCB
hsa04726: Serotonergic synapse	3.14	GABRB2, PRKCB, KCNJ5, PLCB4, ALOX15B, HTR7, SLC18A2, PLA2G4F, GNG2, HTR1D, HTR3A, GNG4, ALOX12, PLA2G4D
hsa04514: Cell adhesion molecules (CAMs)	2.81	ICAM1, NTNG1, NTNG2, CLDN10, CD40, HLA-DMB, CDH4, HLA-G, NCAM2, ITGA8, NLGN4X, PECAM1, CNTN1, HLA-DOA, CD6, ICOSLG
hsa04921: Oxytocin signalling pathway	2.66	ADCY4, ADCY2, CACNG8, CACNB1, CACNB4, KCNJ12, TRPM2, KCNJ14, PRKCB, KCNJ5, KCNJ4, PLCB4, RYR1, PLA2G4F, NFATC1, PLA2G4D
hsa04080: Neuroactive ligand-receptor interaction	2.43	F2RL2, C5AR1, GABRB2, GRIK2, GRIN1, GABBR1, GRIK5, LPAR3, GRIA3, GRIN3B, P2RX5, GRM4, SSTR2, ADRB1, S1PR1, CHRM4, CHRNA9, SSTR1, GRIN2D, HTR7, CHRNA5, ADRA1A, CALCRL, HTR1D, CHRNA3, GRID1, MTNR1A
hsa04024: cAMP signalling pathway	2.39	ADCY4, HCN2, ADCY2, GRIN1, GABBR1, ATP1A3, GRIN3B, GRIA3, TNNI3, GLI1, SSTR2, ADRB1, SSTR1, PDE4A, GRIN2D, PIK3R5, HTR1D, HCAR2, NFATC1
hsa04020: Calcium signalling pathway	2.37	SLC8A3, ADCY4, SLC8A2, ADCY2, CACNA1I, GRIN1, PRKCB, P2RX5, PLCB4, ADRB1, ATP2A3, GRIN2D, HTR7, CACNA1G, RYR1, ADRA1A, PLCD1
hsa04014: Ras signalling pathway	2.32	FGF19, FGF5, FLT4, FGF17, EFNA3, GRIN1, FGF11, PRKCB, RASAL1, HTR7, RASGRP2, PLA2G4F, PLA1A, GNG2, PIK3R5, NGFR, SYNGAP1, GNG4, RASA4, PLA2G4D, NGF
Pathways with downregulated genes		
Pathway	*Benjamini*	*Genes*
hsa05322: Systemic lupus erythematosus	6.65	HIST1H2AB, C7, HIST1H4L, HIST1H2AG, C6, HIST1H2AE, HIST1H2BO, HIST2H2AB, HIST1H2BM, HIST1H4A, HIST1H2BL, HIST1H2BI, HIST2H2AC, HIST1H2BJ, H2AFX, HIST3H2BB, HIST1H4I, HIST1H4J, HIST2H3A, HIST1H3J, HIST1H2BB, HIST1H2BC,

		HIST1H2BE, HIST1H2BF, HIST1H2BG, HIST1H2BH, ACTN2, HIST2H3C, HIST2H3D, HIST2H2BF, HIST1H3A, HIST1H3B, HIST1H2AI, HIST1H2AH, HIST1H3C, HIST1H3E, HIST1H2AJ, HIST1H3F, HIST1H2AM, HIST1H3G, HIST1H2AL, HIST1H3H, HIST1H3I
hsa00140: Steroid hormone biosynthesis	6.43	HSD3B2, CYP3A4, CYP3A5, CYP3A7, HSD3B1, CYP11A1, HSD17B1, UGT1A9, CYP7A1, UGT2B11, UGT2B4, HSD17B6, UGT2B10, UGT2A3, SULT1E1, UGT2B15, AKR1D1, CYP19A1
hsa00053: Ascorbate and aldarate metabolism	5.37	UGT1A9, UGT2B11, RGN, UGT2B4, UGT2B10, UGT2A3, UGT2B15
hsa04610: Complement and coagulation cascades	5.10	KNG1, F11, PLAT, MBL2, C7, MASP2, F13A1, C6, F9, C4BPB, C4BPA, F13B, F3, KLKB1, SERPINA5, SERPIND1, CPB2
hsa00040: Pentose and glucuronate interconversions	5.02	UGT1A9, KL, AKR1B10, UGT2B11, UGT2B4, UGT2B10, UGT2A3, UGT2B15
hsa05034: Alcoholism	4.92	HIST1H2AB, HIST1H4L, HIST1H2AG, HIST1H2AE, HIST1H2BO, HIST2H2AB, HIST1H2BM, HIST1H4A, HIST1H2BL, HIST1H2BI, HIST2H2AC, HIST1H2BJ, H2AFX, HIST3H2BB, HIST1H4I, HIST1H4J, HIST2H3A, HIST1H3J, HIST1H2BB, HIST1H2BC, HIST1H2BE, HIST1H2BF, HIST1H2BG, HIST1H2BH, FOSB, HIST2H3C, HIST2H3D, HIST2H2BF, NTRK2, HIST1H3A, HIST1H3B, HIST1H2AI, HIST1H2AH, HIST1H3C, HIST1H3E, HIST1H2AJ, HIST1H3F, HIST1H2AM, HIST1H3G, HIST1H2AL, HIST1H3H, HIST1H3I
hsa00982: Drug metabolism - cytochrome P450	4.88	GSTA1, CYP3A4, GSTA2, CYP3A5, ALDH3B2, ADH1B, ADH1A, FMO5, UGT1A9, FMO1, ADH4, UGT2B11, UGT2B4, UGT2A3, UGT2B10, UGT2B15
hsa00830: Retinol metabolism	4.86	CYP3A4, CYP3A5, UGT1A9, CYP3A7, ADH4, UGT2B11, ADH1B, UGT2B4, CYP26A1, HSD17B6, ADH1A, UGT2B10, UGT2A3, UGT2B15, RDH5
hsa05204: Chemical carcinogenesis	4.40	GSTA1, CYP3A4, GSTA2, CYP3A5, CYP3A7, NAT2, ADH1B, ALDH3B2, ADH1A, CYP3A43, UGT1A9, ADH4, UGT2B11, UGT2B4, UGT2A3, UGT2B10, UGT2B15
hsa00983: Drug metabolism - other enzymes	4.05	CYP3A4, UGT1A9, NAT2, UGT2B11, UGT2B4, UGT2B10, UGT2A3, UGT2B15, TK1
hsa00980: Metabolism of xenobiotics by cytochrome P450	3.92	GSTA1, CYP3A4, CYP3A5, GSTA2, ALDH3B2, ADH1B, ADH1A, UGT1A9, ADH4, UGT2B11, UGT2B4, UGT2A3, UGT2B10, UGT2B15
hsa04110: Cell cycle	3.01	CDC6, CDK1, PKMYT1, TTK, CDC20, ESPL1, PTTG1, MCM2, CDC25C, CCNB1, CDKN1C, MAD2L1, CCNB2, PLK1, CDKN2C, BUB1, BUB1B, CCNA2
hsa04114: Oocyte meiosis	2.61	CCNB1, CDK1, MAD2L1, CCNB2, PLK1, SGO1, BUB1, FBXO43, PKMYT1, AURKA, ESPL1, CDC20, PTTG1, CDC25C
hsa05202: Transcriptional misregulation in cancer	2.36	PLAT, HIST2H3A, NFKBIZ, HIST1H3J, MMP9, MMP3, HIST2H3C, HIST2H3D, HHEX, EYA1, CDKN2C, HIST1H3A, HIST1H3B, HIST1H3C,

		HIST1H3E, HIST1H3F, HIST1H3G, HIST1H3H, HIST1H3I

Table S4. Upregulated and downregulated KEGG pathways, Related to Figure 2.

Ensembl ID	***Gene***	***Log_2FC***	***padj***
ENSG00000197444	OGDHL	1.08547769	3.29E-30
ENSG00000166411	IDH3A	0.74709247	7.70E-20
ENSG00000204370	SDHD	0.3777972	0.0003
ENSG00000100412	ACO2	0.26021698	0.002
ENSG00000146701	MDH2	0.23945724	0.0009
ENSG00000073578	SDHA	-0.1593416	0.03
ENSG00000138413	IDH1	-0.1812103	0.03
ENSG00000168291	PDHB	-0.2026402	0.02
ENSG00000131828	PDHA1	-0.2107741	0.01
ENSG00000163541	SUCLG1	-0.2111892	0.006
ENSG00000143252	SDHC	-0.2414483	0.02
ENSG00000150768	DLAT	-0.2619025	0.0003
ENSG00000091483	FH	-0.4936542	1.01E-12
ENSG00000014641	MDH1	-0.5085681	3.36E-13
ENSG00000101365	IDH3B	-0.5405112	5.07E-13
ENSG00000067829	IDH3G	-0.5829934	1.14E-09
ENSG00000100889	PCK2	-0.5852916	3.07E-18
ENSG00000131473	ACLY	-0.6074454	9.80E-24
ENSG00000173599	PC	-0.9409933	3.13E-37
ENSG00000182054	IDH2	-1.0677314	8.52E-45

Table S5. [Dysregulated genes in the TCA Cycle KEGG pathway], Related to Figure 2.

Ensembl ID	***Gene***	***Log_2FC***	***padj***
ENSG00000147614	ATP6V0D2	3.973933876	9.35E-140
ENSG00000198763	ND2	1.473526224	2.53E-06
ENSG00000198888	ND1	1.363322749	6.19E-05
ENSG00000198840	ND3	1.217622162	2.54E-33
ENSG00000212907	ND4L	1.095495883	0.0001
ENSG00000198886	ND4	0.866690501	0.002
ENSG00000114573	ATP6V1A	0.803262336	2.80E-32
ENSG00000198804	COX1	0.656245362	1.17E-09
ENSG00000198899	ATP6	0.634543196	0.009
ENSG00000198938	COX3	0.632275024	2.80E-10
ENSG00000171130	ATP6V0E2	0.589272395	2.52E-11
ENSG00000198727	CYTB	0.557687429	0.02
ENSG00000047249	ATP6V1H	0.506014583	5.94E-13
ENSG00000117410	ATP6V0B	0.479535962	2.58E-11
ENSG00000147416	ATP6V1B2	0.437789019	5.51E-09
ENSG00000128609	NDUFA5	0.381648881	0.0008
ENSG00000204370	SDHD	0.377797199	0.0003
ENSG00000198712	COX2	0.322901415	0.005
ENSG00000073578	SDHA	-0.159341647	0.04
ENSG00000023228	NDUFS1	-0.210017339	0.002
ENSG00000112695	COX7A2	-0.211631763	0.02
ENSG00000156467	UQCRB	-0.2162753	0.03
ENSG00000167792	NDUFV1	-0.222597617	0.007
ENSG00000135390	ATP5MC2	-0.222831627	0.002
ENSG00000143252	SDHC	-0.24144827	0.02
ENSG00000160194	NDUFV3	-0.242343108	0.004
ENSG00000131100	ATP6V1E1	-0.274149444	2.61E-05
ENSG00000189043	NDUFA4	-0.277227615	0.0001
ENSG00000176340	COX8A	-0.278696825	0.001
ENSG00000165264	NDUFB6	-0.28300413	0.005
ENSG00000213619	NDUFS3	-0.29075047	0.001
ENSG00000178741	COX5A	-0.297956503	9.27E-05
ENSG00000110719	TCIRG1	-0.300385483	0.002
ENSG00000090266	NDUFB2	-0.301527793	0.001
ENSG00000174886	NDUFA11	-0.318594422	0.001
ENSG00000169021	UQCRFS1	-0.319382279	2.33E-05
ENSG00000130414	NDUFA10	-0.320916351	3.89E-05
ENSG00000131143	COX4I1	-0.336149045	2.75E-07
ENSG00000158864	NDUFS2	-0.343567449	4.23E-06
ENSG00000139180	NDUFA9	-0.357605693	0.0006
ENSG00000004779	NDUFAB1	-0.360587197	2.52E-05
ENSG00000184076	UQCR10	-0.375287362	3.00E-06
ENSG00000116459	ATP5PB	-0.379803823	9.50E-08
ENSG00000126267	COX6B1	-0.388197692	3.84E-08
ENSG00000100554	ATP6V1D	-0.405728961	7.75E-08
ENSG00000131495	NDUFA2	-0.419069805	1.65E-06
ENSG00000115286	NDUFS7	-0.422028053	0.0002
ENSG00000136888	ATP6V1G1	-0.428892928	2.02E-09
ENSG00000183648	NDUFB1	-0.432392964	0.0003
ENSG00000154518	ATP5MC3	-0.445435152	1.00E-08
ENSG00000125356	NDUFA1	-0.459056555	2.84E-07
ENSG00000179091	CYC1	-0.468189203	1.54E-09

ENSG00000127540	UQCR11	-0.475454692	4.04E-09
ENSG00000110955	ATP5F1B	-0.49393262	1.83E-16
ENSG00000099795	NDUFB7	-0.509075592	1.10E-09
ENSG00000168653	NDUFS5	-0.520875625	8.23E-11
ENSG00000159720	ATP6V0D1	-0.540902137	6.67E-12
ENSG00000147123	NDUFB11	-0.542107011	1.51E-08
ENSG00000178127	NDUFV2	-0.542969651	0.006
ENSG00000124172	ATP5F1E	-0.574462256	1.96E-13
ENSG00000152234	ATP5F1A	-0.606022757	1.10E-17
ENSG00000140990	NDUFB10	-0.613088113	6.15E-12
ENSG00000119013	NDUFB3	-0.65837698	2.66E-11
ENSG00000169020	ATP5ME	-0.663226048	5.18E-18
ENSG00000159199	ATP5MC1	-0.712677613	1.05E-19
ENSG00000241468	ATP5MF	-0.735984185	1.21E-15
ENSG00000099624	ATP5F1D	-0.737422752	3.56E-17
ENSG00000169429	CXCL8	-0.820462236	3.09E-17
ENSG00000164405	UQCRQ	-0.860634282	1.66E-38
ENSG00000198695	ND6	-0.979723775	1.42E-08
ENSG00000143882	ATP6V1C2	-1.543440061	0.005

Table S6. [Dysregulated genes in the Oxidative Phosphorylation KEGG pathway], Related to Figure 2

Ensembl ID	Gene symbol	mRNA expression fold change	5hmC fold change
ENSG00000181418	DDN	3.57	-2.84
ENSG00000105131	EPHX3	2.38	-3.82
ENSG00000086619	ERO1B	1.65	4.05
ENSG00000147408	CSGALNACT1	1.33	3.09
ENSG00000149927	DOC2A	1.26	-2.49
ENSG00000142156	COL6A1	1.24	3.13
ENSG00000137752	CASP1	0.98	2.44
ENSG00000119900	OGFRL1	0.71	2.21
ENSG00000145247	OCIAD2	0.71	3.02
ENSG00000183044	ABAT	-1.26	3.04
ENSG00000144395	CCDC150	-1.50	3.36
ENSG00000167874	TMEM88	-2.02	3.60

Table S7. [Promoter regions of genes with both altered mRNA expression and enrichment of 5hmC], Related to Figure 7.

Transparent methods

Differentiation of pluripotent human stem cells to hepatocyte-like cells and induction of intracellular lipid accumulation

Human female H9 pluripotent stem cells (PSCs) were differentiated to hepatocyte-like cells (HLCs) as previously described (Wang et al., 2017). Unless otherwise stated, compounds for this protocol were purchased from Thermo Fisher. Briefly, H9 cells were cultured on Laminin 521 coated plates, with mTeSR1 media, which contained 10 μM ROCK inhibitor. H9s were initially differentiated to an endoderm phenotype in RPMI 1640 media containing 100 ng/mL Activin A (R & D Systems), and 50 ng/mL Wnt3A (Peprotech). Endodermal cells were then differentiated to a hepatoblast phenotype by culturing in Knockout DMEM, containing 20% Knockout Serum Replacement. Finally, cells were differentiated to a HLC phenotype by culturing in HepatoZYME media containing 10 ng/mL hepatocyte growth factor (Peprotech), 20 ng/mL oncostatin M (Peprotech), and 10 μM hydrocortisone 21-hemisuccinate (Sigma Aldrich), until day 17, at which point the cells were used for the assays described in this manuscript.

HLCs were cultured in a 96-well format for measurements of lipid accumulation and in a 6-well format for all other analyses. Each well is a separate differentiation event and represents a biological replicate. Intracellular lipid accumulation was induced in HLCs, as previously described (Lyall et al., 2018). Briefly, at day 17, HLCs were incubated in HepatoZYME media only (controls) or HepatoZYME media containing a cocktail of sodium l-lactate (L; 10mM), sodium pyruvate (P; 1 mM) and octanoic acid (O; 2 mM) (Sigma, Gillingham, UK) (LPO) for a period of 48 hours. For isotopic tracing studies, lactate was replaced with $^{13}C_3$-lactate (CK Isotopes, CLM-1579-05). For mechanistic studies, HLCs were exposed to either 5-Aminoimidazole-4-carboxamide-1-β-D-ribofuranosyl 5′-monophosphate (AICAR; 1mM; Sigma-Aldrich, A1393-50MG), O-(Carboxymethyl)hydroxylamine hemihydrochloride (AOA; 100 μM ; Sigma-Aldrich, C13408-1G) or AICAR combined with monomethyl fumarate (50 μM; Sigma-Aldrich, 651419-1G) for the same duration as LPO.

Cell mitochondrial stress test assay

The oxygen consumption rate (OCR) of LPO-exposed HLCs was measured using the Agilent Seahorse XF Cell Mito Stress Test Kit (Agilent, 103015-100) on a Seahorse XF Analyser (Agilent, California, USA). Data were collected from two separate plates, with each well representing a biological replicate and each plate representing a technical replicate. Analyses were performed under basal conditions and following treatment with oligomycin A (an ATPase inhibitor), carbonyl-cyanide-4-(trifluoromethoxy) phenylhydrazone (FCCP; an ETC uncoupler), and combined rotenone and antimycin A (inhibitors of complex I and III, respectively). Two concentrations of FCCP (0.5 µM and 1.0 µM) were used for optimisation. Since replicates within each group responded similarly to each other, results were combined. OCR was normalised to total protein for each well, using the sulforhodamine B (SRB) assay, as previously described (Orellana and Kasinski, 2016), but with spectrophotometric measurements read at 540 nm.

Citrate synthase assay

Citrate synthase activity was assessed as a readout of mitochondrial integrity (Boutagy et al., 2015; Short et al., 2005). Mitochondria were isolated using the Mitochondria Isolation Kit for Cultured Cells (Thermo Scientific, 89874), as per the manufacturer's instructions, selecting option A for isolation. Citrate synthase activity, a marker of mitochondrial integrity, was then measured using the Citrate Synthase Activity Colorimetric Assay Kit (BioVision, K318), as per the manufacturer's instructions.

Protein Extraction

Adherent HLCs were washed once with ice-cold PBS, before incubating in ice-cold RIPA Lysis and Extraction Buffer (Thermo Scientific, 89900) supplemented with cOmplete Protease

Inhibitor Cocktail tablets (1/10 mL buffer; Roche, 11697498001). The suspended HLCs were placed on ice for 30 minutes, vortexing every 3 minutes, before centrifuging for 20 min at 4 °C, 12,000 rpm. The supernatant was collected and stored at -80 °C until needed.

Western blot analysis

Protein quantification was performed using the Qubit Protein Assay Kit (Invitrogen, Q33211), as per the manufacturer's instructions. Protein concentration was measured using a Qubit Fluorometer (Invitrogen, Massachusetts, USA). Equal concentrations (50 µg) of HLC protein extract in 4 x Sample Loading Buffer (Li-Cor, 928-40004) were loaded onto NuPAGE 4-12% Bis-Tris Protein Gels (Invitrogen, NP0326BOX). Following resolution, protein was transferred to a methanol-activated polyvinylidene difluoride (PVDF) membrane. Protein transfer was measured using Revert 700 Total Protein Stain Kit (Li-Cor, 926-11010) as per the manufacturer's instructions. To enable probing with different antibodies, membranes were then sliced (images shown in Figure S1), blocked with Tris-buffered saline containing Tween 20 (TBST) and 5% skimmed milk powder, and incubated with either Pyruvate Dehydrogenase (staining total α1 and α2 subunits) (C54G1) Rabbit mAb (Cell Signaling Technology, 3205) or SDHA (D6J9M) XP Rabbit mAb (Cell Signaling Technology, 11998), both a 1:1000 dilution. The membranes were washed in TBST before incubating with the secondary antibody, IRDye 680RD Donkey anti-Mouse IgG (Li-Cor, 926-68072) at a 1:10,000 dilution, for 1 h at room temperature, in the dark, with shaking. Blots were visualised on a Li-Cor Odyssey CLx (Li-Cor, Nebraska, USA), and bands normalised to the Revert 700 Total Protein Stain, as per the manufacturer's instructions.

RNA-seq analysis

Total RNA was extracted from HLCs using the Monarch® Total RNA Miniprep Kit (New England BioLabs, T2010). RNA integrity was assessed using a Bioanalyzer (Agilent) with the RNA 6000 Nano kit. All samples had a RIN value >7.0. mRNA sequencing was performed on 3 biological replicates per group by the Beijing Genomics Institute (BGI) (Shenzhen, China).

Library preparation was performed with the TruSeq Stranded mRNA Library Preparation kit (Illumina, RS-122-2101), with additional use of the Ribo-Zero Gold rRNA Removal Kit (Illumina, MRZG12324). Paired-end sequencing was performed on an Illumina HiSeq 4000, with each sample sequenced to a depth >60 million reads. The generated FASTQ files were trimmed to remove adapters, using Trimmomatic (version 0.36) (Bolger et al., 2014), before performing quality control with FastQC (version 0.11.4) (Andrews). Alignment was performed against the *Homo sapiens* GRCh19 assembly. The assembly was first indexed using STAR (version 2.5.1b) before mapping trimmed reads, using STAR (version 2.5.1b) in paired-end mode with default behaviour (Dobin and Gingeras, 2015). Duplicate reads were removed using Picard (version 2.7.11) (2018), before using featureCounts to generate raw read counts for each gene. Differential gene expression (DEG) analysis was performed using DESeq2 (Love et al., 2014). Heatmaps were generated with Heatmapper (Babicki et al., 2016). Pathway enrichment analysis was performed using the Kyoto Encyclopedia of Genes and Genomes (KEGG) function (Kanehisa, 2019; Kanehisa and Goto, 2000; Kanehisa et al., 2019) of the Database for Annotation, Visualization, and Integrated Discovery (DAVID) (Huang et al., 2009a, 2009b).

Real-time quantitative PCR

RNA was taken from that prepared for RNA-sequencing. cDNA was generated using the High Capacity cDNA Reverse Transcriptase Kit (Applied Biosystems, 4368814). A master mix was prepared using PerfeCTa FastMix II (Quanta Biosciences, Inc., 95118-250). cDNA was amplified and quantified using the Universal Probe Library (Roche, Burgess Hill, UK) system on a Roche LightCycler 480 (Roche Diagnostics Ltd, Switzerland). Primer sequences and Universal Probe Library probes are detailed in Table S1.

For quantifying mitochondrial and nuclear DNA, we purified DNA using the Monarch® Genomic DNA Purification Kit (NEB, USA), as per the manufacturer's instructions. DNA was quantified by using the Luna® Universal qPCR Master Mix (NEB, USA) on a Roche

LightCycler 480 (Roche Diagnostics Ltd, Switzerland). Primer sequences and Universal Probe Library probes are detailed in Table S2.

NMR Spectroscopy

This protocol was previously described by Hollinshead *et al* (Hollinshead et al., 2018). At the conclusion of tracer experiments, cells were washed with 2 mL ice-cold 0.9% saline solution and quenched with 0.3 mL pre-chilled methanol (-20 °C). After adding an equal volume of ice-cold HPLC-grade water containing 1 µg/mL D6-glutaric acid (C/D/N Isotopes Inc), cells were collected with a cell scraper and transferred to tubes containing 0.3 mL of chloroform (-20 °C). The extracts were shaken at 1400 rpm for 20 min at 4 °C and centrifuged at 16,000 x g for 5 min at 4 °C. Then, 0.3 mL of the upper aqueous phase was collected and evaporated in eppendorfs, under a vacuum using a Savant™ SpeedVac™ Concentrator (ThermoFisher). These samples were used either for NMR spectroscopy of for GC-MS. For NMR, dried samples were re-suspended in 60 µL of 100 mM sodium phosphate buffer (pH 7.0) containing 500 µM DSS and 2 mM Imidazole, 10% D20, pH 7.0. Samples were vortexed, sonicated (5-15 min) and centrifuged briefly, before transferred to 1.7 mm NMR tubes using an automated Gilson. One-dimensional (1D)-^{1}H NMR spectra and two-dimensional (2D)-^{1}H,^{13}C Heteronuclear Single Quantum Coherence Spectroscopy (HSQC) NMR spectra were acquired using a 600 MHz Bruker Avance III spectrometer (Bruker Biospin) with an inverse cryogenic probe for 1.7 mm NMR sample tubes, fitted with a z-axis pulsed field gradient, at 300 K. Spectral widths were set to 13 and 160 ppm for the ^{1}H and ^{13}C dimensions, respectively. For the indirect (^{13}C) dimension of the 2D-^{1}H,^{13}C HSQC NMR spectra, 1228 out of 4096 (30%) data points were acquired using a non-uniform sampling scheme. ^{13}C-^{13}C splittings were enhanced 4-fold in the ^{13}C dimension. Each sample was automatically tuned, matched and then shimmed (1D-TopShim) to a DSS line width of <1 Hz before acquisition of the first spectrum. Total experiment time was ~15 min per sample for 1D-^{1}H NMR spectra and 1 h per sample for 2D-^{1}H,^{13}C HSQC NMR spectra. 1D-^{1}H NMR spectra were processed using the

MATLAB-based MetaboLab software (Ludwig and Günther, 2011). All 1D data sets were apodized using a 0.3 Hz exponential window function and zero-filled to 131,072 data points before Fourier Transformation. The chemical shift was calibrated by referencing the DSS signal to 0 ppm. 1D-^{1}H NMR spectra were manually phase corrected. Baseline correction was achieved using a spline function (Ludwig and Günther, 2011). 1D-^{1}H-NMR spectra were exported into Bruker format for metabolite identification and concentration determination using Chenomx 7.0 (Chenomx INC). 2D-^{1}H,^{13}C HSQC NMR spectra were reconstructed using compressed sensing in the MDDNMR and NMRpipe software (Delaglio et al., 1995; Kazimierczuk and Orekhov, 2011; Orekhov and Jaravine, 2011). The final spectrum size was 922 real data points for the ^{1}H dimension and 16,384 real data points for the ^{13}C dimension. Analysis was performed using MetaboLab and pyGamma software was used in multiplet simulations (Smith et al., 1994). The methyl group of lactate was used to calibrate the chemical shift based on its assignment in the human metabolome database (Wishart et al., 2013).

GC-MS

Dried polar metabolites were purified as described for NMR spectroscopy. These were derivatised by incubating with 40 µL 2% methoxyamine hydrochloride (Sigma Aldrich, 226904) in pyridine (Thermo Fisher Scientific, 25104) at 60 °C for 1 h, followed by incubation with 60 µL *N*-methyl-*N*-*tert*-butyldimethylsilyltrifluoroacetamide with 1% *tert*-butyldimethylchlorosilane (MTBSTFA with 1% t-BDMCS) at 60 °C for 1 h.

GC-MS analysis was performed using an Agilent 6890GC in combination with an Agilent 5975C MS. The MS was operated under electron impact ionization at 70 eV with the source held at 230 °C and the quadrupole at 150 °C. Helium was used as the carrier gas and maintained at a flow rate of 1 mL/min. 1 µL of derivatised sample was injected (splitless) with an inlet temperature of 280 °C on to a Rxi-5MS column (Restek) The oven temperature was held at 100 °C for 1 min then increased at a rate of 5 °C/min up to a maximum temperature of

330 °C. Ions were detected using selected ion monitoring (SIM) mode as previously described (Battello et al., 2016). MetaboliteDetector software was used to correct for the natural isotope distribution and to determine the mass isotopomer distribution (MID) (Hiller et al., 2009).

DNA hydroxymethylation immunoprecipitation and sequencing (hmeDIP-sequencing)

DNA was purified using the Monarch® Genomic DNA Purification kit (New England BioLabs, T3010S). DNA immunoprecipitation and sequencing was performed as previously described, using the Ion Proton platform (Thomson et al., 2015), with the addition of an IgG control (Merck, 12-370). We validated the DNA immunoprecipitation protocol on Roche LightCycler 480 (Roche Diagnostics Ltd, Switzerland), using the primer sets described in Table S3. We sequenced three biological replicates per group. A mean read length of 137-147 base pairs and 21,130,039 - 31,693,844 reads per sample was achieved. Reads were aligned to the hg19 genome using Torrent Suite v5.2.0. Aligned reads were sorted using SAMtools, before calling peaks using MACS2 (v. 2.1.1) -f BAM --broad --broad-cutoff 0.05 -B -g hs, over corresponding inputs (Zhang et al., 2008). To detect differentially hydroxymethylated regions (DHRs), we used Diffbind with DESeq2 (Stark and Brown). For Diffbind analysis, data were normalised to a pooled input for each group and an IgG control. DHMRs were assigned to genes and other genomic features using the HOMER (v. 4.8; hg19) annotatePeaks tools (Heinz et al., 2010). For candidate hmeDIP analysis, the concentration of each sample was extrapolated from a standard curve of arbitrary concentrations and normalised to 10% input. Regions of interest were identified from the hmeDIP-sequencing dataset. Primers were designed using the NCBI primer-BLAST software (Table S2). Data are available through the Gene Expression Omnibus (GSE144955). Sliding window profiles and heatmaps were generated using deepTools (Ramírez et al., 2014), using the plotProfile and plotHeatmap functions, respectively, with blacklisted regions subtracted.

High content analysis microscopy

Cells were stained with a cell painter assay, adapted from Lyall *et al* and Bray *et al* (Bray et al., 2016; Lyall et al., 2018). Cells were fixed with 50 µL/well 4% (wt/vol) paraformaldehyde (Electron Microscopy Sciences, 15710-S) for 15 minutes at room temperature. For permeabilisation, cells were incubated in 0.1% Triton X-100 (Sigma-Aldrich, T8787) in PBS for 15 minutes at room temperature. For lipid droplet analysis, cells were then stained with a combination of NucBlue Live ReadyProbes® Reagent (2 drops/mL) (Molecular Probes, R37605), HCS CellMask™ Red (2 µL/10 mL) (Invitrogen, H32712), and BODIPY™ 493/503 (1:1000) (Life Sciences, D3922), as per the manufacturer's instructions. Following staining, images were acquired using an Operetta High Content Analysis microscope (Perkin Elmer, Buckinghamshire, UK). Lipid droplet morphology was analysed as previously described (Lyall et al., 2018).

Statistical analysis

All statistical analyses were performed using Graph Prism Version 8.0 for Windows or macOS, GraphPad Software, La Jolla California USA, www.graphpad.com. Normality of data distribution was measured using the Shapiro-Wilks test. Where indicated, data were analysed by unpaired Student's t-test, Mann-Whitney test, one-way analysis of variance (ANOVA) or two-way ANOVA. Data were considered to be significant where $p < 0.05$.

References

Andrews, S. FastQC: a quality control tool for high throughput sequence data.

Babicki, S., Arndt, D., Marcu, A., Liang, Y., Grant, J.R., Maciejewski, A., and Wishart, D.S. (2016). Heatmapper: web-enabled heat mapping for all. Nucleic Acids Res. *44*, W147–W153.

Battello, N., Zimmer, A.D., Goebel, C., Dong, X., Behrmann, I., Haan, C., Hiller, K., and Wegner, A. (2016). The role of HIF-1 in oncostatin M-dependent metabolic reprogramming of hepatic cells. Cancer Metab. *4*, 3.

Bolger, A.M., Lohse, M., and Usadel, B. (2014). Trimmomatic: A flexible trimmer for Illumina sequence data. Bioinformatics *30*, 2114–2120.

Boutagy, N.E., Pyne, E., Rogers, G.W., Ali, M., Hulver, M.W., and Frisard, M.I. (2015). Isolation of mitochondria from minimal quantities of mouse skeletal muscle for high throughput microplate respiratory measurements. J. Vis. Exp. *2015*.

Bray, M.A., Singh, S., Han, H., Davis, C.T., Borgeson, B., Hartland, C., Kost-Alimova, M., Gustafsdottir, S.M., Gibson, C.C., and Carpenter, A.E. (2016). Cell Painting, a high-content image-based assay for morphological profiling using multiplexed fluorescent dyes. Nat. Protoc. *11*, 1757–1774.

Delaglio, F., Grzesiek, S., Vuister, G.W., Zhu, G., Pfeifer, J., and Bax, A. (1995). NMRPipe: A multidimensional spectral processing system based on UNIX pipes. J. Biomol. NMR *6*, 277–293.

Dobin, A., and Gingeras, T.R. (2015). Mapping RNA-seq Reads with STAR. Curr. Protoc. Bioinforma. *51*, 11.14.1-11.14.19.

Heinz, S., Benner, C., Spann, N., Bertolino, E., Lin, Y.C., Laslo, P., Cheng, J.X., Murre, C., Singh, H., and Glass, C.K. (2010). Simple Combinations of Lineage-Determining Transcription Factors Prime cis-Regulatory Elements Required for Macrophage and B Cell Identities. Mol. Cell *38*, 576–589.

Hiller, K., Hangebrauk, J., Jäger, C., Spura, J., Schreiber, K., and Schomburg, D. (2009). Metabolite detector: Comprehensive analysis tool for targeted and nontargeted GC/MS

based metabolome analysis. Anal. Chem. *81*, 3429–3439.

Hollinshead, K.E.R., Munford, H., Eales, K.L., Bardella, C., Li, C., Escribano-Gonzalez, C., Thakker, A., Nonnenmacher, Y., Kluckova, K., Jeeves, M., et al. (2018). Oncogenic IDH1 Mutations Promote Enhanced Proline Synthesis through PYCR1 to Support the Maintenance of Mitochondrial Redox Homeostasis. Cell Rep. *22*, 3107–3114.

Huang, D.W., Sherman, B.T., and Lempicki, R.A. (2009a). Bioinformatics enrichment tools: Paths toward the comprehensive functional analysis of large gene lists. Nucleic Acids Res. *37*, 1–13.

Huang, D.W., Sherman, B.T., and Lempicki, R.A. (2009b). Systematic and integrative analysis of large gene lists using DAVID bioinformatics resources. Nat. Protoc. *4*, 44–57.

Kanehisa, M. (2019). Toward understanding the origin and evolution of cellular organisms. Protein Sci. *28*, 1947–1951.

Kanehisa, M., and Goto, S. (2000). KEGG: Kyoto Encyclopedia of Genes and Genomes. Nucleic Acids Res. *28*, 27–30.

Kanehisa, M., Sato, Y., Furumichi, M., Morishima, K., and Tanabe, M. (2019). New approach for understanding genome variations in KEGG. Nucleic Acids Res. *47*, D590–D595.

Kazimierczuk, K., and Orekhov, V.Y. (2011). Accelerated NMR spectroscopy by using compressed sensing. Angew. Chemie - Int. Ed. *50*, 5556–5559.

Love, M.I., Huber, W., and Anders, S. (2014). Moderated estimation of fold change and dispersion for RNA-seq data with DESeq2. Genome Biol. *15*, 550.

Ludwig, C., and Günther, U.L. (2011). MetaboLab - advanced NMR data processing and analysis for metabolomics. BMC Bioinformatics *12*, 366.

Lyall, M.J., Cartier, J., Thomson, J.P., Cameron, K., Meseguer-Ripolles, J., O'Duibhir, E., Szkolnicka, D., Villarin, B.L., Wang, Y., Blanco, G.R., et al. (2018). Modelling non-alcoholic fatty liver disease in human hepatocyte-like cells. Philos. Trans. R. Soc. B Biol. Sci. *373*, 20170362.

Orekhov, V.Y., and Jaravine, V.A. (2011). Analysis of non-uniformly sampled spectra with multi-dimensional decomposition. Prog. Nucl. Magn. Reson. Spectrosc. *59*, 271–292.

Orellana, E., and Kasinski, A. (2016). Sulforhodamine B (SRB) assay in cell culture to investigate cell proliferation. Bio-Protocol *6*.

Ramírez, F., Dündar, F., Diehl, S., Grüning, B.A., and Manke, T. (2014). DeepTools: A flexible platform for exploring deep-sequencing data. Nucleic Acids Res. *42*, W187-91.

Short, K.R., Bigelow, M.L., Kahl, J., Singh, R., Coenen-Schimke, J., Raghavakaimal, S., and Nair, K.S. (2005). Decline in skeletal muscle mitochondrial function with aging in humans. Proc. Natl. Acad. Sci. U. S. A. *102*, 5618–5623.

Smith, S.A., Levante, T.O., Meier, B.H., and Ernst, R.R. (1994). Computer Simulations in Magnetic Resonance. An Object-Oriented Programming Approach. J. Magn. Reson. Ser. A *106*, 75–105.

Stark, R., and Brown, G. Differential Binding Analysis of ChIP-Seq Peak Data.

Thomson, J.P., Fawkes, A., Ottaviano, R., Hunter, J.M., Shukla, R., Mjoseng, H.K., Clark, R., Coutts, A., Murphy, L., and Meehan, R.R. (2015). DNA immunoprecipitation semiconductor sequencing (DIP-SC-seq) as a rapid method to generate genome wide epigenetic signatures. Sci. Rep. *5*, 9778.

Wang, Y., Alhaque, S., Cameron, K., Meseguer-Ripolles, J., Lucendo-Villarin, B., Rashidi, H., and Hay, D.C. (2017). Defined and scalable generation of hepatocyte-like cells from human pluripotent stem cells. J. Vis. Exp. e55355–e55355.

Wishart, D.S., Jewison, T., Guo, A.C., Wilson, M., Knox, C., Liu, Y., Djoumbou, Y., Mandal, R., Aziat, F., Dong, E., et al. (2013). HMDB 3.0-The Human Metabolome Database in 2013. Nucleic Acids Res. *41*, D801-7.

Zhang, Y., Liu, T., Meyer, C.A., Eeckhoute, J., Johnson, D.S., Bernstein, B.E., Nussbaum, C., Myers, R.M., Brown, M., Li, W., et al. (2008). Model-based analysis of ChIP-Seq (MACS). Genome Biol. *9*, R137.

(2018). Picard Tools - By Broad Institute.